### Geometric frustration of hard-disk packings on cones

#### Jessica H. Sun

Harvard John A. Paulson School of Engineering and Applied Sciences, Harvard University, Cambridge, Massachusetts 02138, USA

#### Abigail Plummer

Princeton Center for Complex Materials, Princeton University, Princeton, New Jersey 08540, USA

#### Grace H. Zhang and David R. Nelson

Department of Physics, Harvard University, Cambridge, Massachusetts 02138, USA

#### Vinothan N. Manoharan \*\*

Harvard John A. Paulson School of Engineering and Applied Sciences, Harvard University, Cambridge, Massachusetts 02138, USA and Department of Physics, Harvard University, Cambridge, Massachusetts 02138, USA



(Received 29 June 2023; accepted 19 September 2023; published 21 November 2023)

Conical surfaces pose an interesting challenge to crystal growth: A crystal growing on a cone can wrap around and meet itself at different radii. We use a disk-packing algorithm to investigate how this closure constraint can geometrically frustrate the growth of single crystals on cones with small opening angles. By varying the crystal seed orientation and cone angle, we find that—except at special commensurate cone angles—crystals typically form a seam that runs along the axial direction of the cone, while near the tip, a disordered particle packing forms. We show that the onset of disorder results from a finite-size effect that depends strongly on the circumference and not on the seed orientation or cone angle. This finite-size effect occurs also on cylinders, and we present evidence that on both cylinders and cones, the defect density increases exponentially as circumference decreases. We introduce a simple model for particle attachment at the seam that explains the dependence on the circumference. Our findings suggest that the growth of single crystals can become frustrated even very far from the tip when the cone has a small opening angle. These results may provide insights into the observed geometry of conical crystals in biological and materials applications.

### DOI: 10.1103/PhysRevE.108.054608

### I. INTRODUCTION

The growth of a crystal can be frustrated by interactions with a curved surface such as a spherical or hyperbolic substrate [1–4]. When the surface has nonzero Gaussian curvature, the frustration stems from variations in the surface metric, which lead to stretching of the crystal lattice. This type of geometrical frustration has been well studied, particularly in colloidal systems [5–13].

Less well studied is frustration arising on surfaces with no Gaussian curvature but on which crystals can form loops, such as cylinders. Although such surfaces do not stretch the lattice, they can nonetheless frustrate a crystal by imposing a closure constraint. As observed in experiments and simulations on colloidal crystals on cylindrical fibers [14], crystals with orientations that are incommensurate with the closure constraint form seams. These seams, which are stable on cylinders but not on flat surfaces unconstrained by periodic boundary conditions, break the translational symmetry of the crystal.

Here we examine how the closure constraint affects crystallization on a cone, which, unlike a cylinder, has a spatially varying circumference. As a consequence, a seam must form with a width that varies in the axial direction whenever the cone angle does not permit the crystal to wrap perfectly around the cone (for a triangular lattice, such commensurate wrappings can be achieved by placing, for example, a 60° disclination at the cone apex). The seam is similar to a tilt grain boundary between two misoriented crystals on a flat substrate [15,16], except that it is a boundary between the misoriented edges of a *single* crystal that has wrapped around the cone. This seam can break both the translational and rotational symmetry of the crystal. We seek to understand how the closure constraint geometrically frustrates crystal growth on a cone.

There are few previous studies of crystallization on a cone. Basin-hopping simulations of colloidal crystals showed that interacting particles on a cone form seams or scar-like defects [17,18]. The aim of these simulations was to understand the defect structure and how it changes with the cone geometry. An experimental study of an atomic system, WS<sub>2</sub>, showed that crystals on a cone form a distinct seam [19]. The cone in this work had a large opening angle, and the size of the

<sup>\*</sup>Corresponding author: vnm@seas.harvard.edu

 $WS_2$  crystal was orders of magnitude larger than the size of the atoms. The main aim of this study was to demonstrate the existence of the seam, which the authors refer to as a tilt grain boundary.

Our aim is to examine the growth process, and in particular how conical crystals grow after closure. In contrast to the basin-hopping simulations [17,18], which reveal energy-minimizing crystal structures, we aim to determine how an out-of-equilibrium growth process leads to disorder. Furthermore, we focus on particles with short-ranged attractions, as seen in previous experimental studies of crystallization on a flat surface [20], sphere [11], and cylinder [14].

To isolate the consequences of geometrical frustration on the crystal structure—and avoid complications associated with multiple nucleation sites and kinetics—we use a greedy algorithm to simulate the idealized growth of a crystal on a conical surface. Our approach, based on an algorithm developed by Bennett to study metallic glasses [21], is inspired by previous work on understanding the effects of geometrical frustration in metallic glasses, and on spherical or hyperbolic surfaces [22,23]. Because we aim to understand effects in the quasi-two-dimensional colloidal systems realized experimentally, we simulate disk packings rather than sphere packings to simplify the computation.

Our simulation is designed to model the slow, reactionlimited growth of a single crystal from a fixed nucleus. Briefly, we initialize the simulation with three disks placed in a triangular configuration with a defined orientation and position on the surface [Fig. 1(a)]. At each subsequent step, the algorithm places a single disk in a position that maximally reduces the energy of the crystal interface. We do not allow the particles to rearrange following placement. On a flat surface, this algorithm produces a perfect crystal. Therefore, any deviation from a perfect crystal on a conical surface is the direct result of geometric frustration, due to a  $\delta$  function of Gaussian curvature at the cone apex [24]. Although this algorithm does not account for the effects of temperature or kinetics, it is a simple and effective way to model the effects of the closure constraint on crystal growth. The details of the method are given in Sec. II.

By modeling crystal growth in this manner, we find a proliferation of defects (defined here as particles with anomalous coordination numbers) for a crystal growing towards the tip of a cone with a small opening angle, as shown in Sec. III. As we shall show, this onset of disorder results from a finite-size effect that depends strongly on the local circumference and is insensitive to the seed orientation and cone angle. Intuitively, the disordered regions appear when a significant fraction of the growing interface consists of the seam of the crystal. We develop a theoretical model that explains the results in Sec. IV A and discuss the influence of the crystal seed location in Sec. IVB [the Appendices provide additional context, including discussions about corrections due to the threedimensional (3D) nature of the particles, commensurate packings on cylinders, and a particularly interesting alternative seed composed of a ring of particles]. We conclude by noting that the transition to a disordered packing can occur surprisingly far from the tip, which may give some insights into the morphology of crystals seen in biology and materials (Sec. V).

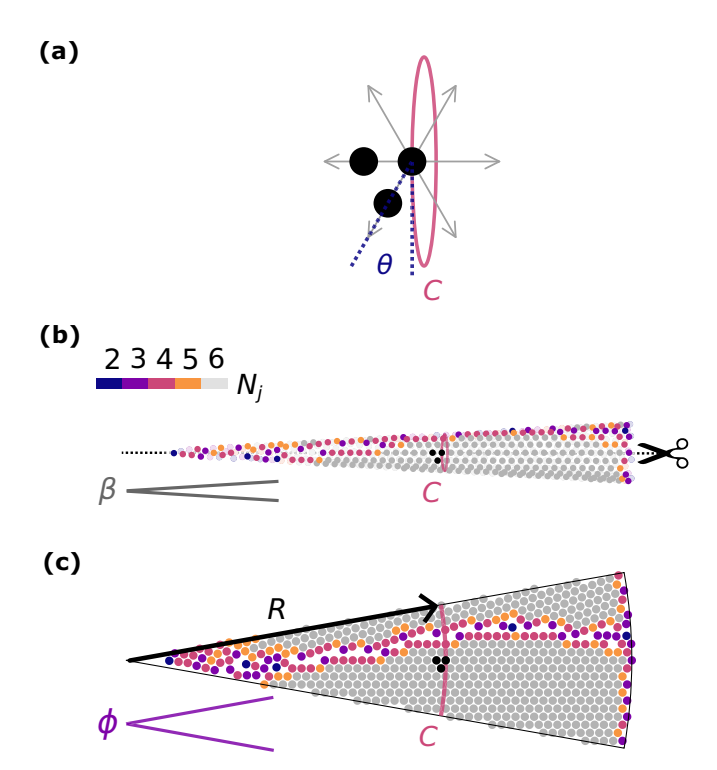


FIG. 1. Geometric parameters in the simulation. (a) Diagram of a triangular crystal seed. The angle  $\theta$  describes the orientation of the lattice vector relative to the red cone circumference curve C. (b) Rendering showing results of a Bennett-type simulation [21] for a 2D packing of disks. We initialize the crystal seed (marked in black) on a 3D cone of angle  $\beta$ . The color of each particle indicates its coordination number  $N_j$ . (c) Rendering showing a mapping of the 3D cone in panel (b) to a 2D unrolled sector of angle  $\phi = 2\pi \sin(\beta/2)$ , where the seed is at a sector radius R from the apex. In this example,  $\theta = 30^{\circ}$ ,  $\phi = 20^{\circ}$ , C = 12  $a_0$  and R = 54.4  $a_0$ . A seam consisting of particles with coordination number  $N_j < 6$  runs in the axial direction.

### II. METHODS

Our algorithm is designed to simulate an idealized crystallization process in which a crystal grows from a single nucleus in a reaction-limited fashion. To create the nucleus, we place three close-packed particles with diameter  $a_0$  in a tangent plane at a radius  $R = C/\phi$  from the sector vertex and with an orientation  $\theta$  with respect to the cone circumference C [Fig. 1(a)]. We then add particles one by one, such that each particle contacts the greatest number of other particles, or, equivalently, forms the greatest number of "bonds." A bond is formed when the centers of two particles are less than  $a_0$  apart with a tolerance of  $10^{-4}a_0$ , representing an interaction potential with a narrow attractive well, as is found in a number of colloidal adsorption experiments [11,14]. If there are several degenerate options for placing the particle, we randomly select one option. We do not place particles such that they form only one bond with the existing assembly because the position of a dangling bond is not well-defined, and a rotation of the dangling bond quickly leads to contact with two particles. We also do not allow any previously placed particles to move, nor do we let the entire crystal translate or rotate.

We choose 2D circular disks of diameter  $a_0$  to represent the effective shapes of 3D spherical particles adsorbed onto a conical surface, and we neglect the anisotropic, position-dependent stretching of particle projections onto a conical surface. This approximation allows us to map the three-dimensional (3D) cone of cone angle  $\beta$  into a flat two-dimensional (2D) circular sector with a periodic boundary condition and a sector angle  $\phi = 2\pi \sin(\beta/2)$ . The mapping is one-to-one because the circumference C of a circular cross-section of the 3D cone [Fig. 1(b)] is equivalent to the arc length C of the 2D sector at a given R [Fig. 1(c)]. The resulting 2D algorithm is computationally simpler, yet is still able to capture the effects of the closure condition on frustration (see Appendix A for a discussion of the limitations of this approach).

We truncate the sector at a radial distance of  $20~a_0$  from the seed position to encourage growth into the sector tip, where we expect to see interesting structures. A simulation terminates when no more particles can be placed into the sector or 1000 particles have been placed. For comparison, the maximum number of particles that can pack into a  $\phi = 5^{\circ}$  sector is around 800.

Since our aim is to understand the effects of geometrical frustration, we select conditions under which perfect triangular crystals cannot form. Perfect crystals lack seams and can form only when the sector angle is a "magic" angle  $\phi = 60^{\circ}P$ , where P is an integer [24–26]. For example, a cylinder is a P = 0 magic cone with  $\phi = 0^{\circ}$ . We therefore restrict our study to cones with  $\phi \neq 60^{\circ}P$ . A seam on such a cone is shown in Figs. 1(b) and 1(c). Particles at the crystal self-boundary have coordination number  $N_j < 6$ . For particles with Lennard-Jones-like pair potentials where the range of attractive interaction is comparable to the defect hard-core diameter, one might expect a grain boundary to form [5]. Our simulations, however, have an interaction range of order  $10^{-4}$  times the hard-core diameter, and the resulting seam, like a stacking fault, maintains its integrity.

We choose to study near-cylindrical cones with small opening angles of  $\phi \leqslant 30^\circ$  to facilitate comparison with results of previous studies of crystals on cylinders [14,27]. When simulating growth on a surface with  $\phi=0^\circ$ , corresponding to a true cylinder, we select a seed orientation  $\theta$  such that seams are still geometrically required.

To characterize the structures, we calculate the bond orientational order parameter  $\psi_{6,j}$  for each particle j with nearest neighbors indexed by k [28,29]:

$$\psi_{6,j} = \frac{1}{N_j} \sum_{k=1}^{N_j} e^{i6\theta_{jk}},\tag{1}$$

where  $\theta_{jk}$  is the angle between the circumferential axis and the vector from particle j to nearest neighbor k, and  $N_j$  is the number of nearest neighbors, or coordination number, of particle j. We consider only particles that are separated by  $a_0 \pm 10^{-4} a_0$  as nearest neighbors.

We also calculate the defect density  $\rho$  as a function of distance R from the vertex. We define defects as particles that have  $|\psi_{6,j}| < 0.9$ . This definition allows us to distinguish defects, which disrupt the order of the crystal, from particles on the boundary of the seam, which are part of an ordered crystal.

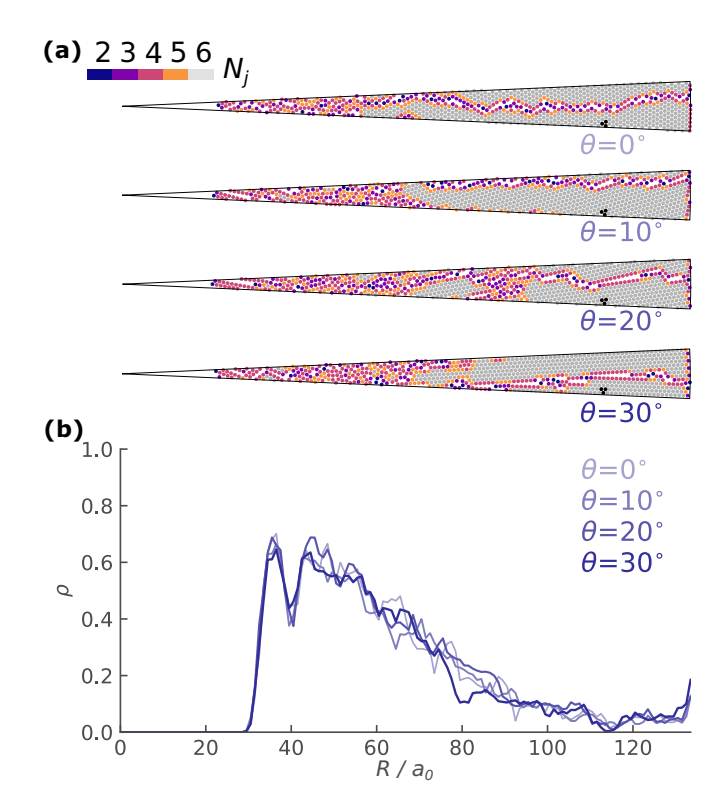


FIG. 2. Variation of particle packings with seed orientation  $\theta$  on cones with sector angle  $\phi$ . (a) Rendering of simulation results at unrolled cone angle  $\phi=5^\circ$  shows that particles in the vicinity of the seed placed at  $R=114.59~a_0~(C=10~a_0)$  are ordered. As the crystal approaches the vertex, the packing becomes disordered. (b) Plot of the defect density  $\rho$  as a function of radial distance R from the tip, where  $\rho$  is the number fraction of particles with  $|\psi_{6,j}|<0.9$  in a given R bin averaged over 100 trials at each seed orientation  $\theta$ . The defect density curves are similar for all  $\theta$  at  $\phi=5^\circ$ . Note that the defect density rises from the seed toward the tip and then drops to zero at  $R\approx28.5~a_0$  because the particles are squeezed out of the tip.

Since the same defect trends are preserved for different cutoff values of  $|\psi_{6,j}|$ , we choose a high cutoff value to obtain a sensitive measure of the defect density (see Appendix B). To calculate the defect density, we first bin the particles by R. We then calculate the number of defects per number of particles within each bin of width  $a_0$ , averaged over 100 trials.

#### III. RESULTS

We first explore the effects of seed orientation on the structure of the system. We find that the crystal initially grows from the seed as an ordered packing of particles, represented by grey particles with  $N_j = 6$  in Fig. 2(a). As the crystal wraps around the cone, it meets itself to form a seam consisting of particles with  $N_j < 6$ . However, as the seam approaches smaller circumferences, these defects begin to dominate the growth interface, leading to the formation of a disordered region consisting primarily of defect particles with  $N_j < 6$  [see Fig. 2(a), regions near tips of cones].

For all seed orientations, the defect density follows a similar curve [Fig. 2(b)], tending to increase as R decreases. The

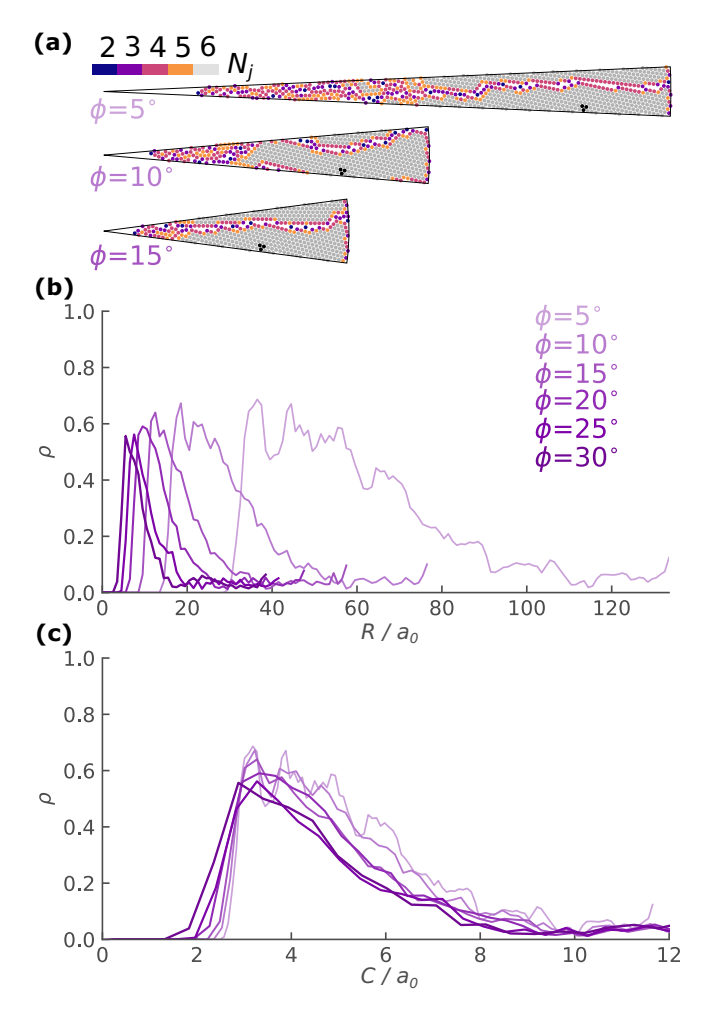


FIG. 3. Variation of particle packings with unrolled sector angle  $\phi$  at fixed seed orientation  $\theta$ . (a) Renderings of simulation results show a long region of  $N_j < 6$  particles at  $\phi = 5^\circ$ , while the disordered regions are concentrated closer to the tip at  $\phi = 10^\circ$  and  $\phi = 15^\circ$ . The seed crystals are at  $C = 10~a_0$  with  $\theta = 40^\circ$ . (b) Plot of the defect density  $\rho$  as a function of R, averaged over 100 trials. The distribution is broad for  $\phi = 5^\circ$  and becomes narrower for increasing sector angles. (c) For each  $\phi$ ,  $\rho$  is mapped to C by  $C = R\phi$ .  $\rho$  collapses as a function of C.

local minimum at approximately  $R=40~a_0$  corresponds to the location where a crystalline cluster three particles wide can form. The defect density then increases again for smaller R, until it reaches a maximum value and falls rapidly to  $\rho=0$  at approximately  $R=28.5~a_0$ . Note that  $R\approx23~a_0$  represents the limit for packing two particles side by side on unrolled cones of angle  $\phi=5^\circ$ . Overall, the tendency of the defect density to increase as the cone narrows suggests that finite-size effects are responsible for the disorder near the tip.

When we initialize crystals on cones with different sector angles with fixed seed orientation  $\theta=40^\circ$ , we find that the position at which the disordered region emerges also varies, as seen for unrolled cones in Fig. 3(a). For small sector angles, we find more disorder farther from the tip, while for larger sector angles, the disordered region is found nearer the tip [Fig. 3(b)]. These results show that cones with small angles can have long disordered regions.

By rescaling R by  $R\phi = C$ , we find that the defect density collapses as a function of cone circumference [Fig. 3(c)]. Defect proliferation therefore depends on the circumference and not strongly on the sector angle or seed orientation. Although the precise sector angle and seed orientation might alter the details of the closure constraint at the single-particle scale, the circumference at which closure occurs has a greater effect on crystal growth.

The density curves do not perfectly collapse because of our discrete binning procedure, which results in a systematic variation with the sector angle. As  $\phi$  increases, the gradient of C also increases. An annular bin of fixed width centered at C will not only access larger circumferences but also have more particles at the larger circumference, which are less likely to be defects. Therefore, at a given C, the defect density for the annular bin is biased towards a lower  $\rho$  as  $\phi$  increases. It is possible that the gradient of C could also affect the defect density in other ways. Nonetheless, the near-collapse of the density curves upon rescaling shows that the circumference, rather than the gradient, is the most important parameter to consider.

To show that defect proliferation can be understood as a function of circumference, we examine crystal growth on cylinders, which have a constant circumference. We find that cylinders with large circumferences have lower defect densities than cylinders with small circumferences [Fig. 4(a)]. For large cylinders, the crystal forms a seam, as expected, and is ordered with few defects. As the circumference decreases, however, the crystal becomes increasingly fragmented as more defects are incorporated into the packing. For thin cylinders, the packing is predominantly disordered.

We find that the defect densities on cylinders as a function of circumference follow the same trend as the defect densities of cones [Fig. 4(b)], provided the orientation  $\theta$  of the triangular seed cluster is not tuned to the special phyllotactic value that allows a commensurate tiling by a triangular crystal [30–32]. Because our focus here is on seeds with random orientations, we neglect the interesting regular tilings that occur for commensurate seed orientations at fixed cylinder radius, or commensurate cylinder radius at fixed seed orientation (Appendix C). For seed orientations  $\theta = 40^{\circ}$ , we find that the defect density distributions appear exponential for small R, regardless of whether the surfaces are conical or cylindrical [Fig. 4(c)]. Crystals on cylinders therefore reproduce the finite-size effects seen in crystals on cones, if special commensurate tilings are ignored [30,31].

### IV. DISCUSSION

#### A. Circumference determines defect density

To provide some intuition for exponential defect proliferation observed in our simulations at small cone circumferences, we introduce a simple theoretical model for slow, reaction-limited growth on a *cylindrical* substrate. We expect our algorithm to simulate slow, reaction-limited growth because particles attach one-by-one to the growing crystal, and each added particle minimizes the local energy of the crystal interface. We use a cylindrical substrate to simplify our theoretical

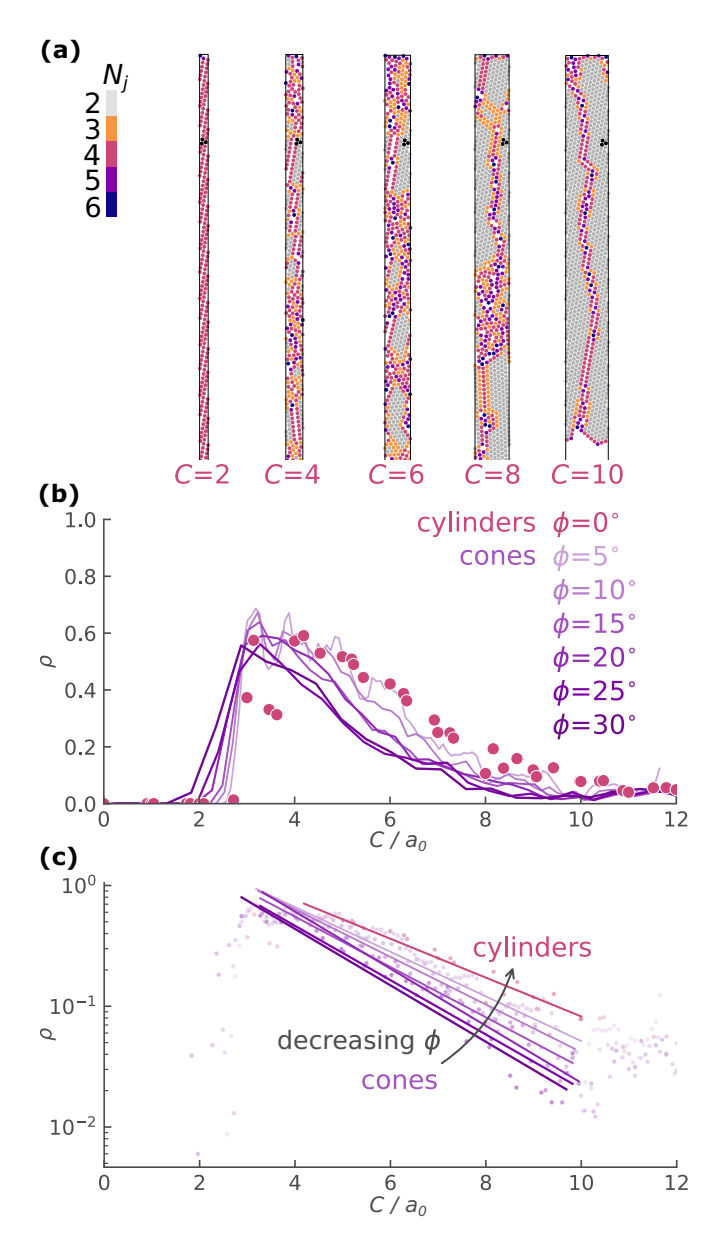


FIG. 4. Particle packings on 2D cylinders of different circumferences, measured in units of the hard core diameter  $a_0$ . (a) Rendering of representative results for simulations. At C=10  $a_0$ , the crystal consists of primarily  $N_j=6$  particles. As C decreases, the crystal becomes fragmented and disordered. The seed orientation is fixed at  $\theta=40^\circ$ . (b) Plot of defect density of cylinders (circles) superimposed on the plot for cones from Fig. 3(c) (lines). The cylinder defect densities are calculated as the number fraction of defects relative to the total number of particles, averaged over 100 trials at each circumference. (c) As the circumference decreases, the defect density grows exponentially at small circumferences for both cones and cylinders. The chosen circumferential values  $C/a_0=2$ , 4, 6, 8, and 10 in this figure do not include any of the special values that would result in perfect packings for  $\theta=40^\circ$  (Appendix C) [32].

arguments because, as shown above, cylinders reproduce the finite-size effects seen on cones.

Given a crystal with a seam and smooth facets as in Fig. 5, we consider the types of lattice sites that an additional particle can diffuse to in the context of a 2D terrace-ledge-kink model,

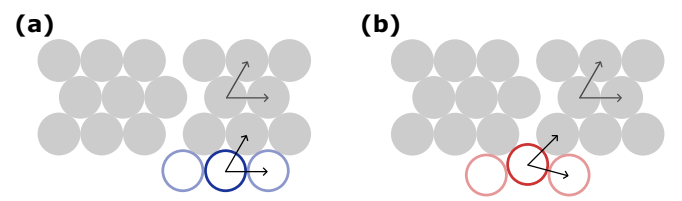


FIG. 5. Illustration of the defect growth process at a seam. Particles in the preexisting crystal are shown as filled gray circles. When all candidate sites result in the formation of two bonds, a particle can attach randomly at (a) a ledge site that initiates a new crystal row or (b) a seam site that creates more sites that break the symmetry of the preexisting crystal. Dark open circles show new particle locations, with lighter open circles emphasizing candidate sites created by attachment of the new particle. Note that this schematic depicts growth on a cylinder—the crystal rows on either side of the seam are parallel.

used to describe ideal surface crystal growth [33]. Particles sitting at the crystalline edges form the ledges where new particles can adsorb. Kinks describe missing particles along the ledge. In our simulation of slow ideal growth, kinks, which have three or more dangling bonds by definition, are higherenergy sites than the smooth ledges, which have two dangling bonds. Therefore, a particle diffusing to the crystal will adsorb to kinks first.

Once the kink sites have been filled, a particle can attach to two types of energetically equivalent lattice sites. The first, a ledge site, is continuous with the preexisting crystal [Fig. 5(a), dark blue circle]. The second, a seam site, is incompatible with the preexisting crystal [Fig. 5(b), dark red circle].

Particle attachment to a ledge site results in on-lattice growth, meaning that the symmetry of the preexisting crystal is preserved. Particle attachment to a seam site results in off-lattice growth, meaning that the symmetry of the preexisting crystal is broken. We expect the density of disordered defects to be related to the proportion of seam sites to ledge sites. Crucially, off-lattice growth increases the probability of further off-lattice growth because adsorption of a seam particle increases the number of off-lattice candidate states overall (light red circles in Fig. 5). Thus, if off-lattice growth is likely, then this argument predicts that it will only become more likely as growth proceeds, initiating the formation of a disordered region as we see in our simulations.

To further develop this simplified picture, we estimate the probability of disordered growth. A perfect crystal with rows composed of  $N_{\rm row}$  particles and a single seam as in Fig. 5 has of order  $N_{\rm row}$  candidate sites that lead to on-lattice growth, and only order one candidate sites that lead to off-lattice growth. Therefore, the probability of on-lattice growth occurring initially is  $P_1(t=0) \sim (1-1/N_{\rm row})$ , and the probability of off-lattice growth is  $P_2(t=0) \sim 1/N_{\rm row}$ . If on-lattice growth occurs,  $P_1$  and  $P_2$  do not change. If off-lattice growth occurs, then we expect that  $P_2$  increases by an amount that scales with  $1/N_{\rm row}$ . If  $P_2$  reaches some threshold value—say  $P_2=1/2$ , at which half of the candidate sites lead to off-lattice growth—runaway off-lattice growth results, leading to the formation of a disordered region.

What is the probability of  $P_2(t)$  increasing to this threshold value? If on-lattice growth occurs following off-lattice

growth, there may be some healing of the disordered seam region, and  $P_2$  may decrease. We therefore make the simplifying approximation that  $P_2$  increases only when off-lattice growth occurs many times in a row, and  $P_2$  increases by  $1/N_{\text{row}}$  every time off-lattice growth occurs consecutively. With these assumptions, the probability of off-lattice growth occurring s consecutive times scales as

$$P_s = P_2(t = 0) P_2(t = 1) \dots P_2(t = s)$$
  
  $\sim \frac{1}{N_{\text{row}}} \times \frac{2}{N_{\text{row}}} \times \dots \times \frac{s}{N_{\text{row}}} = \frac{s!}{(N_{\text{row}})^s}.$  (2)

To find the probability that  $P_2$  reaches 1/2, we let  $s = N_{\text{row}}/2$  and make Stirling's approximation:

$$P_{N_{\text{row}}/2} = \frac{(N_{\text{row}}/2)!}{(N_{\text{row}})^{N_{\text{row}}/2}} \sim \frac{\sqrt{N_{\text{row}}}}{2^{N_{\text{row}}/2}} e^{-N_{\text{row}}/2}.$$
 (3)

Therefore, this simple model predicts that the probability of a disordered region initiating increases exponentially as the number of particles in a crystal row encircling the cylinder decreases. The predicted exponential scaling is consistent with the simulation results, which show that the defect density increases exponentially with decreasing circumference [Fig. 4(c)]. The same argument can explain defect formation on a cone, albeit with some subtleties, which we discuss in Appendix D.

#### B. Seeds close to the tip

These results, all of which concern seeds placed far from the tip of the cone, raise the question of whether placing seeds closer to the tip of the cone might help prevent disorder near the tip. We therefore examine simulations of crystallization with seeds placed at different circumferences.

We find that while crystals seeded far from the tip (at  $C=9\ a_0$ ) are able to grow normally towards the tip until the onset of disorder, crystals that are seeded closer to the tip (at  $C=7\ a_0$  and  $C=5\ a_0$ ) first form a small crystal before disorder emerges [Fig. 6(a)]. The formation of these small crystals is reflected in the defect density, which shows a dip at the circumference corresponding to the seed location for all seeds placed at  $C<9\ a_0$  [Fig. 6(b)].

We can explain these results using the model from Sec. IV A. A crystal grows until the closure constraint demands formation of a seam. But when the crystal is seeded near the tip, the circumference is small, and hence  $N_{\text{row}}$  is small. Therefore, off-lattice growth is more probable at these small circumferences, and the crystal becomes frustrated a short distance from the seed.

Interestingly, in some cases we see that new crystals can form at the wider part of the cone, as shown in the  $C=7\ a_0$  example. However, these new crystals quickly become frustrated again as new seams and grain boundaries form. Consequently, the defect density dips at the circumference of the seed and then rises with increasing circumference, until it exceeds the defect density for a seed placed at  $C=10\ a_0$  [Fig. 6(b)]. We conclude that crystals that are seeded near the tip can temporarily escape the finite-size effect leading to disorder near the tip, though at the expense of increased disorder farther from the seed site.

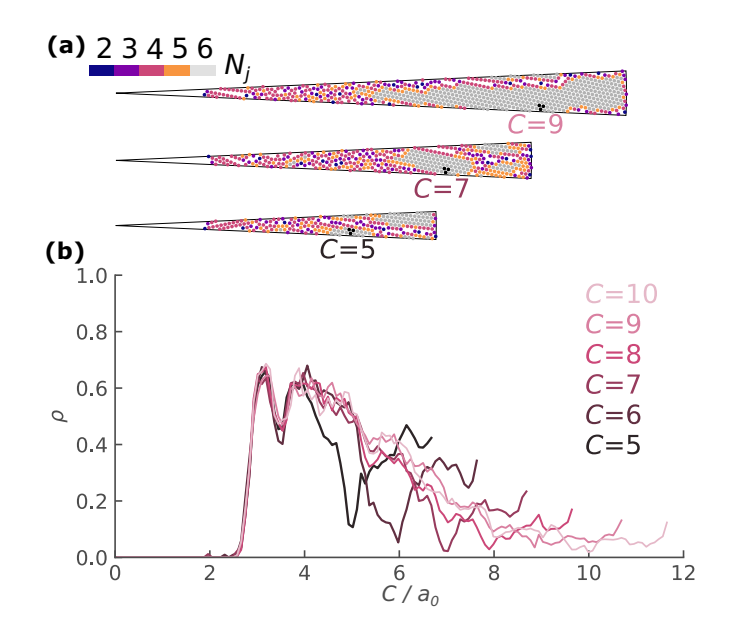


FIG. 6. Particle packings on sectors initialized at different seed positions. (a) Rendering of simulation results for  $\phi = 5^{\circ}$  with seed positions at C = 5  $a_0$ , C = 7  $a_0$ , and C = 9  $a_0$  and a seed orientation of  $\theta = 40^{\circ}$ . (b) Plot of the defect density  $\rho$  as a function of C, averaged over 100 trials. Crystals seeded at small circumferences have dips in the defect density that correspond to the seed location.

#### V. CONCLUSION

We have shown that crystal growth on a cone is geometrically frustrated. For any nonmagic cone angle, a seam is required. A disordered region forms near the tip because defects tend to appear at the seam, and the probability of these defects proliferating increases exponentially as the circumference decreases.

This type of frustration has implications for slow, reactionlimited crystal growth on cones. Near-cylindrical cones have long sections in which defects form with high probability, resulting in large areas of potentially disrupted crystallization. In wider cones, the increase in defect probability is concentrated at the tip and can block tip closure, leading to holes at the tips of conical shells.

These results may help explain tip-closure problems observed in experimental systems. For example, the conical capsids of HIV often exhibit large holes at the tip [26]. Also, crystals of WS<sub>2</sub> have been found to terminate unexpectedly far from the tip [19]. Future experiments on colloidal systems, such as the system described in Chapter 6 of Ref. [34], might shed light on whether tip-closure failures are the result of the frustration mechanism revealed by our simulations.

Our results also show that control over nucleation may be crucial to fabricating conical crystals for applications. Disordered regions form near the tip of the crystal, regardless of whether the seed is far or close to the tip. But a crystal seeded near the tip can temporarily bypass the finite-size effect, resulting in a locally reduced defect density. Therefore, if the surface or interactions can be controlled such that nucleation occurs close to the tip, then at least small crystals can be formed in this region. Furthermore, if the geometry of nucleation can be controlled, new crystalline structures might

be realized experimentally. In Appendix E, we discuss how a nucleus consisting of a ring of particles might grow, and how the size of the resulting crystal depends on the elastic modulus.

Our simulations used a greedy algorithm because our aim was to reveal the geometric frustration faced by crystals growing on a conical surface. Our simulations do not account for kinetics, thermal fluctuations, or vibrational entropy. Future simulations and experiments are therefore needed to develop a more complete physical understanding of conical crystal growth. Nonetheless, our results show that, apart from the special case of magic-angle cones, any conical crystal is subject to geometrical frustration that promotes disorder at small circumferences.

Data for the simulations are openly available on the Harvard Dataverse [35]. Code for the simulations is available under the GNU General Public License v3 at Ref. [36].

#### ACKNOWLEDGMENTS

We thank Lara Braverman for insightful conversations. This research was primarily supported by the National Science Foundation through the Harvard University Materials Research Science and Engineering Center under Grant No. DMR-2011754. Additional support was provided by the National Science Foundation Graduate Research Fellowship Program under Grants No. DGE-2140743 and No. DGE-1745303.

### APPENDIX A: 3D CORRECTIONS TO EFFECTIVE PARTICLE SHAPE

Using a constant particle shape simplifies our analysis considerably. However, a position-dependent particle shape would more accurately model 3D spheres assembling onto a cone. Though we do not consider these corrections in this work, we describe them briefly here.

To provide intuition, we first consider two circular particles tangent to each other and to the surface of a circle, as shown in Fig. 7. The distance between particle centers is  $d_{\rm ctr} = 2 \ a_0$ . However, measured along the surface, the distance between the two points at which the particles touch the substrate is

$$d_{\text{surf}} = 2R \sin^{-1} \left( \frac{a_0}{R + a_0} \right)$$

$$\approx 2 a_0 - \frac{2 a_0^2}{R} + \mathcal{O}\left( \frac{a_0^3}{R^2} \right). \tag{A1}$$

In the limit  $a_0/R \rightarrow 0$ ,  $d_{\rm ctr} = d_{\rm surf}$ , while for finite R,  $d_{\rm surf} < d_{\rm ctr}$ . This difference can be significant: for R=3  $a_0$ ,  $d_{\rm surf}$  is approximately 75% of  $d_{\rm ctr}$ , for example. We can represent this 2D assembly in 1D by "unwrapping" the circle to form a line segment of length  $2\pi R$  with periodic boundaries, upon which we place two adjacent line segments of length  $d_{\rm surf}$ . The dimensional reduction creates an effective particle size that depends on the surface curvature.

This idea can be straightforwardly extended to a cylindrical substrate with radius R, as described in Memet  $et\ al.$  [37]. Two adjacent particles aligned with the axial direction

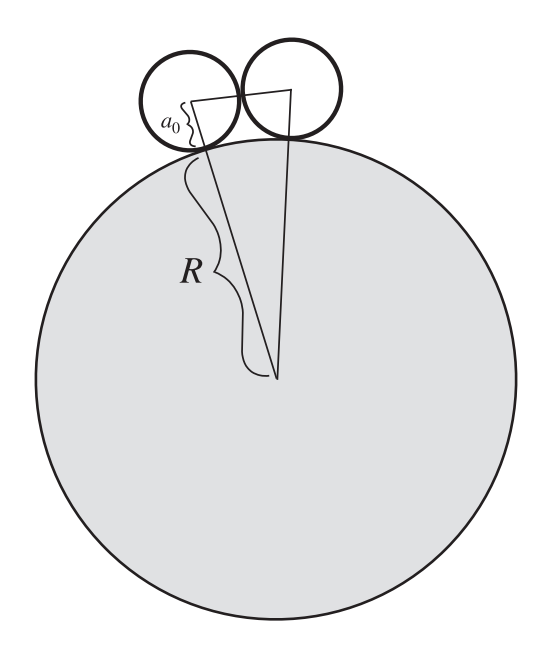


FIG. 7. Diagram showing that the distance between particles along a surface differs from 2  $a_0$  when the surface is curved

are separated by a distance  $d_{\rm ctr}$ , while two adjacent particles aligned with the circumferential direction are separated by a distance  $d_{\rm surf}$  measured along the surface. Upon unwrapping the cylinder to form a flat 2D domain with periodic boundaries, we find that the effective particle shape is an extended, ellipse-like shape. When centered at the origin of the xz plane, this effective shape is described by the equation

$$(a_0 + R)^2 \sin^2(x/R) + z^2 = a_0^2.$$
 (A2)

Note that this is the equation of a circle in the limit  $R \gg a_0$ , as expected. Thus, we can simulate crystallization on a cylinder using a flat 2D domain while taking into account the 3D shape of the particles if we generalize our algorithm to use the oblong shapes given by Eq. (A2) instead of circles.

For a cone, the effective particle shape is more complicated. Far from the cone tip, curvature effects will be small, and the effective particle shape will be approximately circular. As we move closer to the tip, curvature along the circumferential direction increases, and the effective particle shape will become more elongated.

We can solve for this position-dependent effective particle shape by considering horizontal slices through the cone and a tangent spherical particle. Effective particle shapes for different locations on the domain are shown in Fig. 8.

Using a position-dependent effective particle shape will likely further disrupt crystallization close to the sector center/apex (where the particle shape is not approximately circular). These 3D effects should be considered by simulations that seek to more accurately model experiments. Though solving explicitly for the effective particle shape in Fig. 8 is useful for estimating the corrections to our model, simulating the assembly process directly in three dimensions would be a more straightforward way to incorporate this effect.

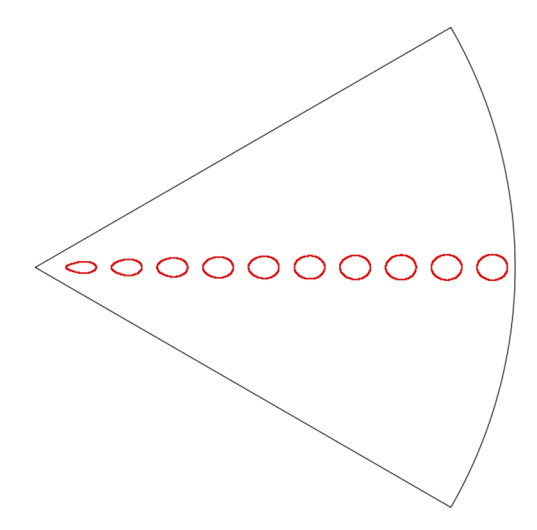


FIG. 8. Diagram showing that the effective particle shape on a cone is a tapered ellipse-like shape, pointing towards the sector center. The correction is much more pronounced close to the tip.

### APPENDIX B: DEFECT DEFINITION

We choose  $|\psi_{6,j}| < 0.9$  to define a defect. We use the bond orientational order instead of the more commonly used definition based on coordination number so that we can filter out dislocations that form along the seam, which have  $|\psi_{6,j}| \geqslant 0.9$ . These dislocations would otherwise contribute a background defect density. Changing the cutoff value from 0.9 does not alter the shape of the defect density distribution, as seen in Fig. 9.

# APPENDIX C: COMMENSURATE PACKINGS ON CYLINDERS

On a cone, perfect crystals can form only when the sector angle is a "magic" angle  $\phi = 60^{\circ}P$ , where P is an integer [24–26]. The only magic angle in the range  $\phi \leq 30^{\circ}$  studied here is  $\phi = 0^{\circ}$ , corresponding to a cylinder. On a cylinder, there are many commensurate packings, depending on the circumference and angle of the crystal. These commensurate packings are determined by a pair of phyllotactic indices

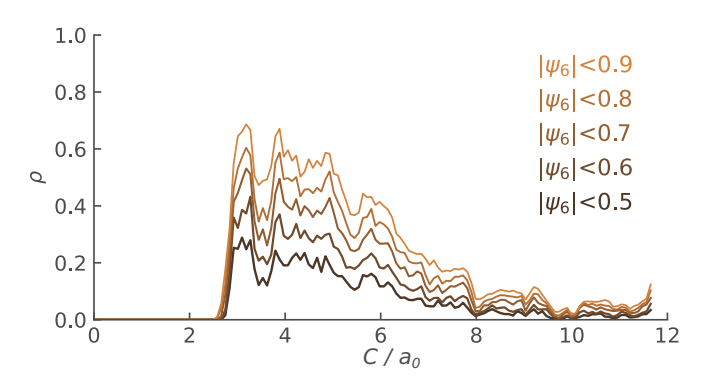


FIG. 9. Plots of defect density for various choices of cutoff for  $|\psi_{6,j}|$ . The simulations were carried out for sectors with  $\phi=5^\circ$  and for seeds initiated at C=10  $a_0$  with orientation  $\theta=40^\circ$ . Each curve is an average over 100 trials.

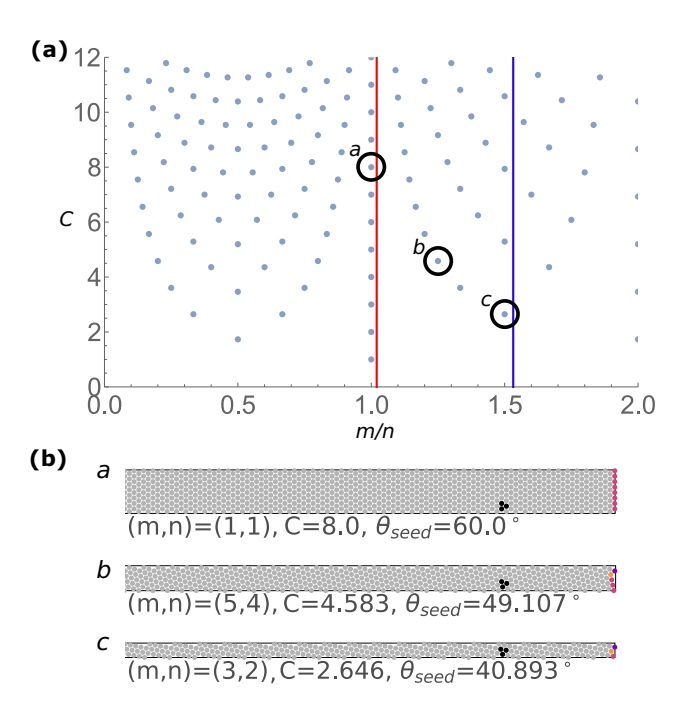


FIG. 10. Commensurate chiral and achiral particle packings on cylinders. (a) Plot of Eq. (C1) which represents the circumferences C and seed orientations  $\theta$  that should result in commensurate packings, where  $\theta$  is related to (m,n) by Eq. (C2). The blue vertical line represents a seed orientation of  $\theta = 40^{\circ}$  as shown in Fig. 4 of the main text, while the red vertical line represents a seed orientation of  $\theta = 59^{\circ}$ , as shown in Fig. 11. Note that the vertical lines do not intersect any commensurate points for  $C < 20 \ a_0$ . Here we show commensurate points for  $C < 12 \ a_0$ , which is the circumference range studied. (b) Renderings of simulation results on an unrolled cylinder with crystal seed parameters set at commensurate points. We observe perfect packings even for chiral seed orientations and small circumferences.

(m, n), where [32]

$$\frac{1}{2\pi}|C| = \frac{a_0}{2\pi}\sqrt{m^2 + n^2 - mn},\tag{C1}$$

and  $a_0$  is the lattice spacing. The integers m and n are related to the crystal orientation by [32]

$$\tan\left(\frac{\pi}{2} - \theta\right) \approx \frac{2}{\sqrt{3}} \left(\frac{m}{n} - \frac{1}{2}\right),$$
 (C2)

where  $\theta$  is the angle between the crystal lattice and circumferential axis.

The commensurate points in the (C, m/n) plane are plotted in Fig. 10(a) according to Eq. (C1). The blue vertical line represents the crystal orientation  $\theta = 40^{\circ}$ . Along this line there are no commensurate packings, at least for  $C < 20 \ a_0$ . The red vertical line represents crystal orientations  $\theta = 59^{\circ}$ . Along this line there are also no commensurate packings for  $C < 20 \ a_0$ . The circled points are visualized in Fig. 10(b). Our simulations are able to reproduce the commensurate packings at the expected phyllotactic values.

When the seed orientation is fixed at a near-commensurate value of  $\theta = 59^{\circ}$ , our simulations reveal interesting nonmonotonic behavior in the defect density plot (Fig. 11). While the

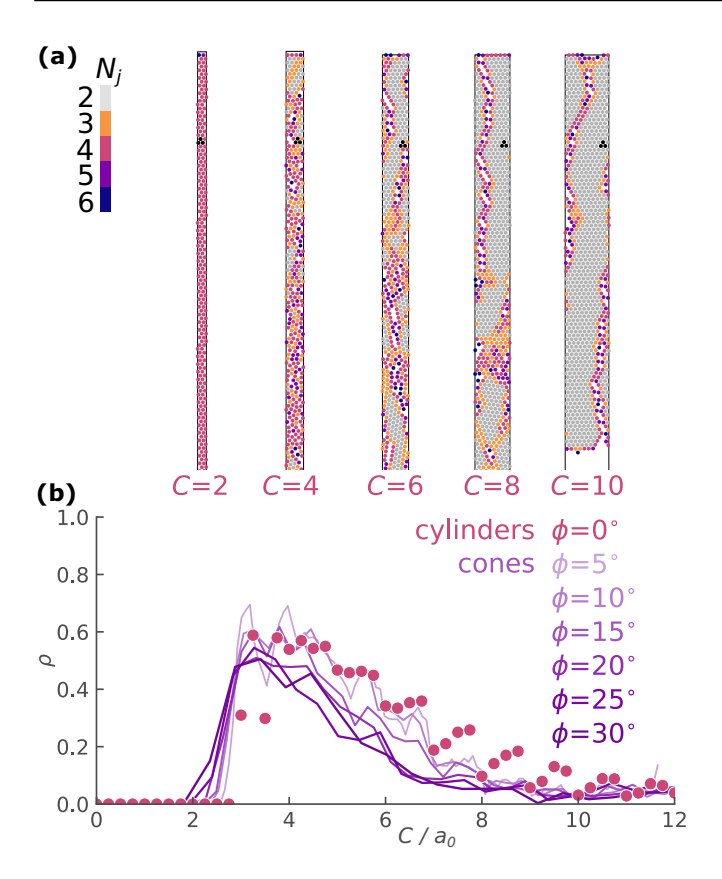


FIG. 11. Nonmonotonic defect density behavior of near-commensurate cylinders. (a) Rendering of representative results for simulations on an unrolled cylinder for seed orientation fixed at  $\theta = 59^{\circ}$ . As C decreases, the crystal becomes fragmented and disordered. (b) Plot of the defect density of cylinders (circles) superimposed on a plot for cones (lines) for simulations fixed at  $\theta = 59^{\circ}$ . Note that the cylinder defect densities are nonmonotonic, with local minima at integer C values.

overall boundary of the sampled defect densities follows the same profile as cones, we observe local dips at integer C values, corresponding to values close to commensurate points [Fig. 10(a)]. Therefore, while cylinders of different crystal orientations manage to capture the general defect density behavior of cones, we choose to analyze seed orientations  $\theta = 40^{\circ}$ , for which we encounter fewer nearby commensurate points as cylinder circumference increases (see blue line in Fig. 10).

# APPENDIX D: CIRCUMFERENCE ARGUMENT APPLIED TO CONES

We now seek to extend the growth probability argument presented in Sec. IV A to a conical substrate. On a cone, crystals grow along conical geodesics. The theory for cylinders might need to be modified if the number of particles along a geodesic interface were to differ significantly from the number of particles that can fit around the cone circumference at a given height, or if the interface/geodesic length were to depend strongly on the crystal orientation.

However, we find that if we restrict our attention to geodesics that represent realistic crystal boundaries (for

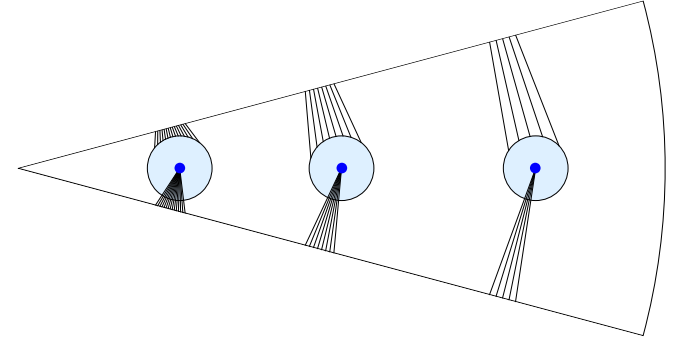


FIG. 12. Diagram showing examples of geodesics on the circular sector that make permissible crystal boundaries. Three possible starting points are shown (blue points) from which geodesics depart toward the bottom at a range of angles, circle the cone once, and return within a distance  $a_0$  of the initial starting point (light blue disk). The lengths of the geodesics that meet these conditions are well-approximated by the circumference of a circular cross-section of the cone at the initial points.

example, the geodesics that start at a particular point on the cone, circle the cone once, and returns to within  $a_0$  of the starting point) on cones with small angles, the length of a geodesic is well-approximated by the circumference of a circular cross-section. The simplest case is a geodesic at an angle  $\theta = 0$ . The geodesic length is  $2R\sin(\phi/2)$ , which is the same as the circumference at that point,  $R\phi$ , in the small-angle limit. Perhaps more surprisingly, varying  $\theta$  leads to only a minor correction. Only a narrow range of  $\theta$  values produce curves that circle the apex one time, returning to within  $a_0$  of their starting point, and these admissible curves are also well-approximated by the circumference, as we show graphically in Fig. 12. It is therefore a reasonable approximation to set  $N_{\text{row}} \approx \text{circumference}/a_0$  and to explain the dependence on circumference (and independence on seed orientation and cone angle) in our cone simulations with our simplified growth model developed for cylinders.

## APPENDIX E: INITIALIZATION WITH A RING OF PARTICLES

In the main text, we investigate crystal growth initiated by a seed of three particles in contact with one another [Fig. 1(a)]. In this Appendix, we provide a brief overview of the interesting effects that occur when a crystal instead nucleates on a ring of particles oriented parallel to the base of the cone (Fig. 13). Such a ring-shaped crystal could be realized experimentally by, for example, milling a shallow trench or placing a metallic ring flush against the conical surface. Reliably creating ring-shaped initial conditions in experiments is the subject of ongoing work.

First, we consider a ring of particles initiating crystal growth on a cylindrical substrate. A crystalline band of any width is not strained on a cylinder provided that the initial seeded ring is commensurate with the circumference of the cylinder. The energy of a crystal of circumference  $C_0$  and width w is given by

$$E_{\text{cylinder}} = E_{\text{bound}} + E_{\text{bulk}},$$
 (E1)

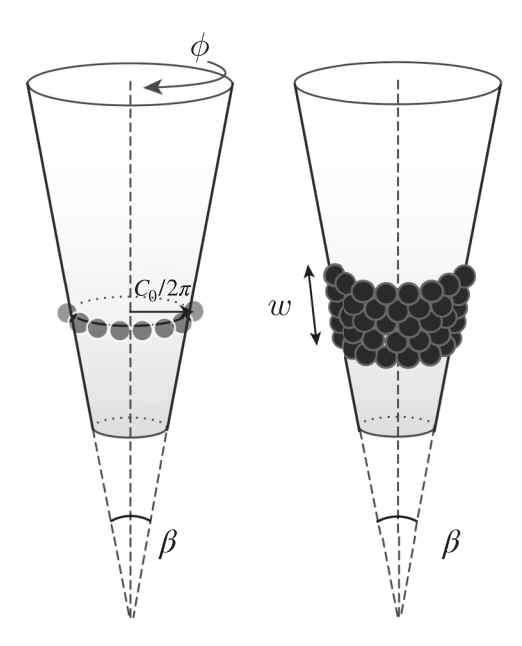


FIG. 13. Schematic of ring initial condition, defining the ring circumference  $C_0$  and the banded crystal width w.

where

$$E_{\text{bound}} = 2\sigma C_0,$$
 (E2)

$$E_{\text{bulk}} = -\Delta f C_0 w, \tag{E3}$$

where  $\sigma$  is the energy per unit length required to form a free boundary in a crystalline bulk by breaking interparticle bonds, and  $\Delta f$  is the change in free energy of the noncrystalline phase relative to the crystalline phase [38]. Note that  $\Delta f>0$  is positive, as the disordered phase has higher energy than the ordered crystalline phase. Since the energy in Eq. (E1) decreases with increasing crystal width w for any w>0, crystal growth always lowers the energy of the system. Therefore, the seeded crystal would nucleate and grow to cover the entire cylindrical surface. Note that the lack of a nucleation barrier here is specific to our ring seeding configuration. An energy barrier is typically present for nucleation from a more isotropic seed on a two-dimensional surface.

In contrast, on the surface of a cone, crystal growth from an initially unstrained ring of particles can generate nonzero elastic strain. In the limit of a small cone angle, a crystalline band of width w centered about an initial commensurate ring of circumference  $C_0$  has energy [39]

$$E_{\rm cone} = E_{\rm bound} + E_{\rm bulk} + E_{\rm strain},$$
 (E4)

where

$$E_{\text{bound}} = 2\sigma C_0,$$
 (E5)

$$E_{\text{bulk}} = -\Delta f C_0 w, \tag{E6}$$

$$E_{\text{strain}} = \frac{Y \tan^2(\pi \sin \beta/2)}{6C_0} w^3, \tag{E7}$$

where  $\beta$  is the cone angle defined in Figs. 1 and 13 and Y is the two-dimensional Young's modulus of the colloidal crystal. Owing to the  $\sim w^3$  scaling of the strain energy in Eq. (E7), the derivative of the total energy E with respect to w becomes positive above a critical width  $w_c$  given by

$$w_c = \frac{2C_0}{\pi \beta} \sqrt{\frac{2\Delta f}{Y}},\tag{E8}$$

indicating the width at which colloidal crystallization is arrested. Note that the nonzero Gaussian curvature of the conic surface, which manifests as the varying circumference of the cone cross-section, is an essential ingredient for this growth arrest.

Interestingly, we can also leverage this crystallization arrest phenomenon to propose an alternative method for measuring the Young's modulus of the colloidal crystal, a quantity that has typically been extracted through various inference methods [11,40]. On inverting Eq. (E8), we have

$$Y = 8\Delta f \left(\frac{C_0}{\pi \beta w_c}\right)^2.$$
 (E9)

Since the critical width of a crystalline band on a cone is a directly measurable quantity, we can use it to infer the Young's modulus *Y* through Eq. (E9).

In this calculation, and throughout the paper, we have assumed that the triangular lattice is the most stable configuration. For longer-ranged interactions, however, it is possible that the crystal could restructure itself to accommodate the elastic strain. Future work might examine whether other lattices, such as the rhombic lattice studied by Mughal and Weaire [31] in the context of disk packings on cylinders, might represent stable structures on the cone.

<sup>[1]</sup> D. R. Nelson, Order, frustration, and defects in liquids and glasses, Phys. Rev. B 28, 5515 (1983).

<sup>[2]</sup> G. M. Grason, Perspective: Geometrically frustrated assemblies, J. Chem. Phys. 145, 110901 (2016).

<sup>[3]</sup> M. F. Hagan and G. M. Grason, Equilibrium mechanisms of self-limiting assembly, Rev. Mod. Phys. **93**, 025008 (2021).

<sup>[4]</sup> F. C. Meldrum and C. O'Shaughnessy, Crystallization in confinement, Adv. Mater. **32**, 2001068 (2020).

<sup>[5]</sup> A. R. Bausch, M. J. Bowick, A. Cacciuto, A. D. Dinsmore, M. F. Hsu, D. R. Nelson, M. G. Nikolaides, A. Travesset, and D. A. Weitz, Grain boundary scars and spherical crystallography, Science 299, 1716 (2003).

<sup>[6]</sup> P. Lipowsky, M. J. Bowick, J. H. Meinke, D. R. Nelson, and A. R. Bausch, Direct visualization of dislocation dynamics in grain-boundary scars, Nat. Mater. 4, 407 (2005).

<sup>[7]</sup> V. Vitelli, J. B. Lucks, and D. R. Nelson, Crystallography on curved surfaces, Proc. Natl. Acad. Sci. USA 103, 12323 (2006).

<sup>[8]</sup> M. Bowick, H. Shin, and A. Travesset, Dynamics and instabilities of defects in two-dimensional crystals on curved backgrounds, Phys. Rev. E 75, 021404 (2007).

<sup>[9]</sup> W. T. M. Irvine, V. Vitelli, and P. M. Chaikin, Pleats in crystals on curved surfaces, Nature (London) 468, 947 (2010).

<sup>[10]</sup> W. T. M. Irvine, M. J. Bowick, and P. M. Chaikin, Fractionalization of interstitials in curved colloidal crystals, Nat. Mater. 11, 948 (2012).

- [11] G. Meng, J. Paulose, D. R. Nelson, and V. N. Manoharan, Elastic instability of a crystal growing on a curved surface, Science **343**, 634 (2014).
- [12] R. E. Guerra, C. P. Kelleher, A. D. Hollingsworth, and P. M. Chaikin, Freezing on a sphere, Nature (London) 554, 346 (2018).
- [13] N. Singh, A. K. Sood, and R. Ganapathy, Observation of two-step melting on a sphere, Proc. Natl. Acad. Sci. 119, e2206470119 (2022).
- [14] N. Tanjeem, W. H. Wilkin, D. A. Beller, C. H. Rycroft, and V. N. Manoharan, Geometrical frustration and defect formation in growth of colloidal nanoparticle crystals on a cylinder: Implications for assembly of chiral nanomaterials, ACS Applied Nano Materials 4, 10682 (2021).
- [15] C. Carraro and D. R. Nelson, Grain-boundary buckling and spin-glass models of disorder in membranes, Phys. Rev. E 48, 3082 (1993).
- [16] V. R. Coffman and J. P. Sethna, Grain boundary energies and cohesive strength as a function of geometry, Phys. Rev. B 77, 144111 (2008).
- [17] M. A. Miller, J. O. Law, A. Finlay Gerrand, and H. Kusumaatmaja, Colloidal clusters on curved surfaces, in *Frontiers of Nanoscience*, edited by D. J. Wales (Elsevier, Amsterdam, Netherlands, 2022), Vol. 21, Chap. 7, pp. 129–150.
- [18] A. Finlay Gerrand, Colloidal Crystals on Conical Surfaces, Ph.D. thesis, Durham University, 2021.
- [19] H. Yu, N. Gupta, Z. Hu, K. Wang, B. R. Srijanto, K. Xiao, D. B. Geohegan, and B. I. Yakobson, Tilt grain boundary topology induced by substrate topography, ACS Nano 11, 8612 (2017).
- [20] J. R. Savage, D. W. Blair, A. J. Levine, R. A. Guyer, and A. D. Dinsmore, Imaging the sublimation dynamics of colloidal crystallites, Science 314, 795 (2006).
- [21] C. H. Bennett, Serially deposited amorphous aggregates of hard spheres, J. Appl. Phys. 43, 2727 (1972).
- [22] M. Rubinstein and D. R. Nelson, Order and deterministic chaos in hard-disk arrays, Phys. Rev. B **26**, 6254 (1982).
- [23] M. Rubinstein and D. R. Nelson, Dense-packed arrays on surfaces of constant negative curvature, Phys. Rev. B 28, 6377 (1983).
- [24] G. H. Zhang and D. R. Nelson, Fractional defect charges in liquid crystals with *p*-fold rotational symmetry on cones, Phys. Rev. E 105, 054703 (2022).

- [25] A. Krishnan, E. Dujardin, M. M. J. Treacy, J. Hugdahl, S. Lynum, and T. W. Ebbesen, Graphitic cones and the nucleation of curved carbon surfaces, Nature (London) 388, 451 (1997).
- [26] B. K. Ganser, S. Li, V. Y. Klishko, J. T. Finch, and W. I. Sundquist, Assembly and analysis of conical models for the HIV-1 core, Science 283, 80 (1999).
- [27] D. A. Wood, C. D. Santangelo, and A. D. Dinsmore, Self-assembly on a cylinder: A model system for understanding the constraint of commensurability, Soft Matter 9, 10016 (2013).
- [28] Y. Han, N. Y. Ha, A. M. Alsayed, and A. G. Yodh, Melting of two-dimensional tunable-diameter colloidal crystals, Phys. Rev. E 77, 041406 (2008).
- [29] B. I. Halperin and D. R. Nelson, Theory of two-dimensional melting, Phys. Rev. Lett. 41, 121 (1978).
- [30] W. F. Harris and R. O. Erickson, Tubular arrays of spheres: Geometry, continuous and discontinuous contraction, and the role of moving dislocations, J. Theor. Biol. **83**, 215 (1980).
- [31] A. Mughal and D. Weaire, Theory of cylindrical dense packings of disks, Phys. Rev. E **89**, 042307 (2014).
- [32] D. A. Beller and D. R. Nelson, Plastic deformation of tubular crystals by dislocation glide, Phys. Rev. E 94, 033004 (2016).
- [33] J. Nozawa, S. Uda, S. Guo, A. Toyotama, J. Yamanaka, J. Okada, and H. Koizumi, Step kinetics dependent on the kink generation mechanism in colloidal crystal growth, Cryst. Growth Des. 18, 2948 (2018).
- [34] N. Tanjeem, Effect of geometry on packing and parking of colloidal spheres, Ph.D. thesis, Harvard University, Cambridge, MA, 2020.
- [35] J. Sun, A. Plummer, G. H. Zhang, D. R. Nelson, and V. Manoharan, Data for "Geometric frustration of hard-disk packings on cones," https://doi.org/10.7910/DVN/ZQ4BUR, Harvard Dataverse, V1 (2023).
- [36] https://github.com/manoharan-lab/cone-disk-packings.
- [37] E. Memet, N. Tanjeem, C. Greboval, V. N. Manoharan, and L. Mahadevan, Random sequential adsorption of spheres on a cylinder, Europhys. Lett. 127, 38004 (2019).
- [38] P. M. Chaikin, T. C. Lubensky, and T. A. Witten, *Principles of Condensed Matter Physics*, Vol. 10 (Cambridge University Press, Cambridge, UK, 1995).
- [39] J. R. Barber, Elasticity, 2nd ed. (Springer, Berlin, 2002), p. 52.
- [40] C. D. Mellor, M. A. Sharp, C. D. Bain, and A. D. Ward, Probing interactions between colloidal particles with oscillating optical tweezers, J. Appl. Phys. 97, 103114 (2005).